Naunyn-Schmiedeberg's Arch Pharmacol (2013) 386:775–787
DOI 10.1007/s00210-013-0868-x

ORIGINAL ARTICLE

Is pannexin the pore associated with the P2X7 receptor?

A. V. P. Alberto · R. X. Faria · C. G. C. Couto · L. G. B. Ferreira · C. A. M. Souza · P. C. N. Teixeira · M. M. Fróes · L. A. Alves

Received: 19 March 2012 / Accepted: 2 April 2013 / Published online: 9 May 2013

Abstract The P2X7 receptor (P2X7R), an ATP-gated cation channel, is expressed predominantly in leukocytes. Activation of P2X7R has been implicated in the formation of a cytolytic pore (i.e., a large conductance channel) that allows the passage of molecules up to 900 Da in macrophages. At least two hypotheses have been presented to explain the conversion of a nonselective cation channel to a cytolytic pore. One hypothesis suggests that the pore is a separate molecular structure activated by P2X7R, and the second asserts that this is an intrinsic property of P2X7R (pore dilation). Based on connexin knockout and hemichannel antagonist studies, some groups have concluded that connexins and pannexins, the hemichannel-forming proteins in vertebrates, are fundamental components of the large conductance channel associated with P2X7R. Dye uptake and electrophysiology experiments were used to evaluate the efficacy and specificity of some hemichannel antagonists under conditions known to open the large conductance channel associated with P2X7R. Hemichannel antagonists and interference RNA (RNAi) targeting pannexin-1 did not affect P2X7R macroscopic currents [ATP, 1,570±189 pA; ATP+100 μM carbenoxolone (CBX), 1,498±100 pA; ATP+1 mM probenecid (Prob), 1,522 ±9 pA] or dye uptake in a FACS assay (ATP, 63±5 %; ATP+100 μM CBX, 51.51±8.4 %; ATP+1 mM Prob, 57.7±4.3 %) in mouse macrophages. These findings strongly suggest that the high-permeability pore evident after prolonged P2X7R activation does not occur through connexin or pannexin hemichannels in murine macrophages. Another membrane protein may be involved in P2X7R pore formation.

Keywords Connexin · Pannexin · Hemichannels · Gap junctions · P2X7 receptor · Gap junction antagonists · Pore · Electrophysiology

Abbreviations

P2X7R	P2X7 receptor
ox-ATP	Adenosine 5′-triphosphate, periodate oxidized sodium salt
CBX	Carbenoxolone
LY	Lucifer yellow
EB	Ethidium bromide
PI	Propidium iodide
18α-GA	18 α-Glycyrrhetinic acid
BBG	Brilliant Blue G
Mef	Mefloquine
Prob	Probenecide
RNAi	Interference RNA
Mac	Macrophage
BSA	Bovine serum albumin
PBS	Phosphate-buffered saline
Panx1	Pannexin-1
Lipof	Lipofectamine

Introduction

P2X7R is a nonselective cation channel that is gated by extracellular ATP (Surprenant et al. 1996) and is responsible

Electronic supplementary material The online version of this article (doi:10.1007/s00210-013-0868-x) contains supplementary material, which is available to authorized users.

A. V. P. Alberto · R. X. Faria · C. G. C. Couto · L. G. B. Ferreira · C. A. M. Souza · P. C. N. Teixeira · L. A. Alves (✉)
Laboratório de Comunicação Celular, Instituto Oswaldo Cruz, Fundação Oswaldo Cruz, FIOCRUZ,
Av. Brasil, 4365 Manguinhos,
CEP: 21045-900, Rio de Janeiro, RJ, Brazil
e-mail: alveslaa@ioc.fiocruz.br

M. M. Fróes
Laboratório de Neuroanatomia Celular, Instituto de Ciências Biomédicas, Universidade Federal do Rio de Janeiro (UFRJ), Rio de Janeiro, Brazil

for the permeabilizing and cytolytic effects of ATP (Cockcroft and Gomperts 1980; Heppel et al. 1985; Steinberg et al. 1987). This receptor exhibits a number of unusual properties, including the ability to change membrane permeability via at least two distinct electrical mechanisms, depending on concentration and time of agonist exposure (Surprenant et al. 1996). Thus, when low concentrations of ATP (<10 μM) are applied for short periods, P2X7R functions as a cation channel that is permeable to monovalent and divalent cations. However, after prolonged exposure (seconds) to high concentrations (>100 μM) of ATP, an ionic channel of high conductance is opened. P2X7R pores are typically defined as large conduits for the transmembrane flow of ions and low molecular weight metabolites, with an upper limit of approximately 900 Da in macrophages (Surprenant et al. 1996; Steinberg et al. 1987). P2X7R pore activation has been implicated in the release of a variety of physiological mediators, such as NADPH, glutamate, and ATP itself (Alloisio et al. 2008; Li et al. 2003; Kim et al. 2007; Marcoli et al. 2008; Gudipaty et al. 2003). P2X7R pores are also permeable to exogenously applied fluorescent dyes, e.g., propidium iodide (PI), YO-PRO1, and ethidium bromide (EB), enabling the investigation of pore formation in many biological preparations (Rassendren et al. 1997a; Faria et al. 2005).

Although classically related to apoptosis (Ferrari et al. 1997; Humphreys et al. 2000) and, more recently, to cell lysis (Virginio et al. 1999a; Auger et al. 2005), activation of P2X7R has been implicated in many other aspects of cell function, including proliferation (Monif et al. 2009) and intercellular signaling. Moreover, structural aspects of cell behavior related to P2X7R activity include actin reorganization during smooth muscle contraction (Cario-Toumaniantz et al. 1998) and bone reabsorption (Ke et al. 2003). Furthermore, it has been suggested that P2X7R pores modulate neurotransmitter release (Atkinson et al. 2004), synaptic vesicle release (Deuchars et al. 2001), and parotid acinar exocrine secretion (Li et al. 2003).

Despite this vast repertoire of effects on cell behavior, the identity of this large conductance pore and the mechanism of its formation have not been determined. Two main hypotheses have been proposed: (1) dilation of the channel portion of the receptor by prolonged exposure and/or high agonist concentrations, leading to the formation of an intrinsic transmembrane pore (Virginio et al. 1999a; Virginio et al. 1999b) and (2) P2X7R activation triggers the opening of a protein pore distinct from the receptor itself (Coutinho-Silva and Persechini 1997; Persechini et al. 1998). Several studies indicate the participation of an accessory pore in P2X7R activation (Faria et al. 2005; Jiang et al. 2005; Pelegrin and Surprenant 2006).

Recently, it has been proposed that pannexin-1 channels (Barbe et al. 2006) are the entities responsible for P2X7R pore-like activity (Pelegrin and Surprenant 2006). Hemichannels are formed in invertebrates by innexins (Bauer et al. 2005) and in vertebrates by connexins and pannexins (Bruzzone et al. 2005). Functional connexin gap junction intercellular channels allow the exchange of ions and molecules up to 1,000 Da. In this arrangement, at the single intercellular channel level, each cell contributes one hemichannel (or connexon in the case of gap junction-forming connexins). The hemichannel is formed by six proteins classically identified as connexins (Bennett et al. 1991; Harris 2001; Evans and Martin 2002). Pannexins exhibit high structural similarity to connexins, with an analogous membrane conformation and oligomeric assembly of subunits, even though there is no molecular homology (Bruzzone and Dermietzel 2006). Unlike connexins, pannexins form functional plasma membrane channels but not gap junction channels; these plasma membrane channels allow the transmembrane passage of molecules up to 900 Da (Bosco et al. 2011; Locovei et al. 2007). In addition to the structural homology between pannexin and connexin, their pharmacological sensitivity profiles are similar, which makes distinctions between their associated pores difficult to determine experimentally (Locovei et al. 2007).

A growing body of recent evidence indicates that connexin hemichannels form transmembrane pores in different cell types, allowing communication between the extracellular and intracellular environments (Valiunas et al. 1999; Valiunas and Weingart 2000; Valiunas 2002; Contreras et al. 2002; Suadicani et al. 2006). These studies suggest a role for hemichannels in both physiological and pathological conditions.

Interestingly, gap junction antagonists such as CBX, flufenamic acid, and quinine derivatives have been shown to inhibit dye uptake and intracellular calcium increase following activation of P2X7R stably transfected in astrocytoma cell lines (Suadicani et al. 2006). This supports recent suggestions that pannexin is involved in P2X7 pore formation.

Strong evidence that pannexin pores play an important role in P2X7R pore-like activity was obtained from pannexin-1 antagonists and anti-pannexin-1 RNAi, which cause a decrease in P2X7 pore formation (Pelegrin and Surprenant 2006). Moreover, coexpression of P2X7R with pannexin in oocytes provided evidence that pannexin channels may be the pore-forming units activated by ATP stimulation of P2X7R (Locovei et al. 2007).

However, there is evidence against hemichannel involvement. Qu et al. (2011) demonstrated that in pannexin-knockout bone marrow-derived macrophages, no blockage of dye uptake was elicited by ATP, suggesting the involvement of proteins other than pannexin hemichannels. We have demonstrated that Cx43KO macrophages, as well as gap junction/hemichannel antagonists such as octanol and heptanol, fail to block ATP-induced LY uptake (Alves et al. 1996). In addition, we showed that heptanol, 18α-GA, and

CBX, another set of gap junction and hemichannel antagonists, did not affect P2X7R-associated pore formation in thymic epithelial cells (Faria et al. 2005). Building on prior reports regarding the actions of hemichannel antagonists on P2X7R-associated pores, we use ionic current analysis and dye uptake assays in mouse and rat macrophages to evaluate the effects of drugs that reduce hemichannel function.

Materials and methods

Animals and experimental design

Male Wistar rats (6 weeks old) and Swiss Webster mice (4 weeks old) weighing approximately 150 and 30 g, respectively, were used. The animals were housed under standard conditions of natural 12 h light and dark cycle at 23±2 °C, relative humidity of 50–60 %, with free access to food and water. The animals were acclimatized for 7 days before use in experiments. Protocols and surgical procedures were approved by the local ethical committee. The animals were cared for in accordance with the Ethical Principles in Animal Experimentation of the Brazilian College of Animal Experimentation. The animals were euthanized by CO_2 asphyxiation from pressurized cylinders while contained in a small plastic chamber.

Chemicals

ATP, ionomycin, oxidized ATP (ox-ATP), Brilliant Blue G (BBG), 18α-glycyrrhetinic acid (18α-GA), carbenoxolone (CBX), lanthanum chloride ($LaCl_3$), flufenamic acid, EB, PI, and Probenecide (Prob) were purchased from Sigma Chemical (St. Louis, MO, USA). Mefloquine (Mef) was acquired from Farmanguinhos (Rio de Janeiro, RJ, Brazil), heptanol was obtained from MERCK (Whitehouse Station, NJ, USA), and trypan blue was acquired from Allied Chemical (Detroit, MI, USA).

Macrophage isolation and culture

Macrophages were obtained from the intraperitoneal space of mice and rats. In brief, cells were plated with RPMI 1640 medium (Sigma Chemical, St. Louis, MO, U.S.A.) in a 96-well plate (Corning, SP, Brazil) or a Petri dish at a density of 2×10^5 cells per well, followed by a 40-min incubation in 5 % CO_2 enriched air at 100 % humidity. To select adherent macrophages, two gentle washes were performed with PBS. After washing, the macrophages were maintained in culture for at least 24 h in RPMI 1640 medium supplemented with 10 % fetal bovine serum (Cultilab, SP, Brazil). After the incubation period, the macrophages were washed again with PBS to remove dead cells.

Dye uptake

Rat and mouse macrophage permeabilization was visualized by the differential uptake of 50 nM EB or PI. Cells were plated in a 96-well plate (Corning, SP, Brazil) and incubated with P2X7R antagonists or gap junction antagonists for 10 min, with the exception of 300 μM ox-ATP, which was incubated for 50 min. After this initial incubation, 5 mM ATP was added, and the cells were incubated for 15 min in the presence of antagonists. During the last 5 min of the ATP incubation, we applied EB. After these procedures, the cells were washed, the medium was replaced with extracellular saline solution, and the cells were imaged by fluorescence microscopy (Nikon, Eclipse TS2000, Tokyo, Japan). The data were analyzed with Image J software, Version 4.02 (National Institutes of Health). Dye uptake was quantified by determining the number of positive cells in a field of 100 cells. The field of 100 cells was chosen arbitrarily. The positive cells displayed red fluorescence under the same conditions used for the negative control (untreated cells). Negative controls were incubated only with propidium iodide, which does not permeate live cells since the membrane was intact. All antagonists were added prior to the addition of ATP in all experiments.

Electrophysiology

Mouse macrophage currents were recorded using a whole-cell configuration of the patch-clamp technique with an Axopatch-1D amplifier (Axon Instruments, San Mateo, CA, USA). All recordings were performed at 37 °C. The cells were transferred to a chamber mounted on a microscope stage (Nikon, Eclipse TS2000, Tokyo, Japan). Patch pipettes were pulled from IBBL borosilicate glass capillaries (1.2 mm, inner filament; World Precision Instruments, New Haven, CT, USA).

A high-resistance seal (1–10 GΩ) was established by gentle suction, and the circumscribed cell membrane was disrupted using additional suction. Currents obtained in the presence of agonist were not corrected for leakage because it was negligible; currents in the absence of agonist were <0.1 % of the maximal agonist induced currents. Currents were recorded after 5–10 min of dialysis of internal solutions. Recordings were included for analysis only when current and membrane conductance returned to within 1–5 % of the control values after agonist washout. This procedure prevents the possibility of considering artifactual current increase through seal leakage or cell lysis.

The holding potential was adjusted to −60 mV, except for the voltage ramps that was −80 mV. The series resistance was 6–10 MΩ for all experiments, and no compensation was applied for currents smaller than 400 pA. Above this level, series resistances were 85 % compensated. Experiments in

which the series resistance increased substantially during the measurement process were discarded. Cell capacitance (12.22±1.01 pF; $n=103$) was measured by applying a 20-mV hyperpolarizing pulse, starting from a holding potential of −20 mV. The capacitive transient was then integrated and divided by the amplitude of the voltage step (20 mV). Cells with access resistance (R_a) values higher than 25 MΩ or varying more than 20 % during the experiment were discarded.

Voltage ramps were applied from −120 to +80 mV over 10 s (16 mV/s) with 40-s intervals between ramps and holding potential of −80 mV between ramps. Currents recorded during voltage ramps were filtered with a corner frequency of 5 kHz (8-pole Bessel filter), digitized at 20–50 kHz using a Digidata 1320 interface (Axon Instruments, Palo Alto, CA, USA), and acquired with a personal computer using pClamp 9 software package. Reversal potentials were then depicted directly from the current–voltage plots.

We have also applied voltage steps, ranging from −120 to +80 mV, with +10 mV increments at 1-s intervals. The step duration was 500 ms with intervals of 1 s each. Steps were assayed before, during, and after the application of the antagonists.

Relative current was defined as the ratio between the peak amplitude of the ionic current and the cell capacitance. The maximal response was defined as the response to ATP alone. All other recordings of antagonists in the presence of ATP were normalized relative to this maximal value.

Drug application

In most of the experiments, drugs were administered using an automatic micropipette with variable volume (Gilson, Villiers-le-Bel, France) by positioning its tip inside the bath solution. After the micropipette was in the bath, we waited a few seconds for stabilization of the baseline before drug application. All drugs were dissolved in saline solution immediately before usage, depending on the protocol. The antagonists (100 μM CBX, 1 mM heptanol, 100 μM 18α-GA, 100 μM $LaCl_3$, and 10 μM BBG) were added 5 min before the application of 1 mM ATP, with the exception of ox-ATP (300 μM 50 min before ATP application). Ion currents were determined for a single application of ATP (from 5 to 30 s) after preincubation with antagonist. Experiments were performed under perfusion (RC-24 chamber, Warner Instrument Corporation, Handem, USA) under constant flow of external solution to confirm the data obtained through micropipette application. Whole-cell patch-clamp recordings were performed using mouse macrophages bathed in an external solution containing the following (mM): 150 NaCl, 5 KCl, 1 $MgCl_2$, 1 $CaCl_2$, and 10 HEPES, pH 7.4. The pipette solution contained the following (mM): 150 KCl, 5 NaCl, 1 $MgCl_2$, 10 HEPES, and 0.1 EGTA, pH 7.4, at room temperature.

FACS analysis

Mouse macrophages were prepared as described previously (Faria et al. 2005). The cells were incubated at 37 °C in a 5 % CO_2 humidified atmosphere.

The cells were stimulated for 15 min in the presence of ATP; 5 μg/mL PI was added during the last 5 min. Some experiments were performed by exposing the cells to antagonists for only 2 min before ATP stimulation. In the FACS analyses, we defined the region between 10^0 and 10^1 as "negative" cells. The M2 region was considered to contain permeabilized cells. This region provided the data shown in the bar graphs. The M3 region represented possible dead cells and was therefore not used to prepare the graphs. All samples were resuspended in FACS buffer (phosphate-buffered saline (PBS +/+, Invitrogen) with 0.5 % bovine serum albumin (BSA, Sigma, fraction V) at a concentration of 10^6 cells/mL. For each sample, 10,000 events were acquired using FACSCalibur (Becton & Dickinson, Mountain View, CA, USA) with CellQuest software (BD Biosciences).

Total RNA extraction

Trizol (1 mL, Invitrogen, California, USA) was added to each culture bottle (75 cm^2) or suspension (5×10^6 mouse macrophages). Samples were then homogenized and incubated for 10 min at room temperature to allow complete dissociation of nucleoprotein complexes. After incubation, nucleic acids were recovered from the lysate by adding 0.2 mL chloroform (Sigma) to each sample and incubating for 5 min at room temperature, followed by centrifugation at 14,000 rpm for 15 min. The aqueous layer was then transferred to a new tube. Nucleic acids were precipitated by adding 0.5 mL isopropanol. The samples were left at room temperature for 10 min and then centrifuged for 10 min at 14,000 rpm. The pellet was washed with 75 % ethanol, homogenized in a vortex, centrifuged for 5 min at 8,000 rpm, and air-dried at room temperature. RNase-free water (20 μL, treated with 0.1 % DEPC and inactivated by autoclaving) was used to resuspend the total RNA.

Reverse transcriptase PCR

Total RNA extracted from mouse macrophages as described above was transcribed with reverse transcriptase (first-strand cDNA kit, Pharmacia Biotechnology). The cDNA obtained was amplified using a pair of primers specific for pannexin-1: forward 5′-CTCTGCTGCTCATCTCGCTG-3′ and reverse 5′-GAGTATGGCAAACAGCAGTAG-3′ (Jacobson et al. 2010). PCR was performed by mixing 2 μg cDNA, 2.0 μM each "primer", 62.5 μM dNTPs, 2 μL PCR buffer, 2.5 mM $MgCl_2$, 0.5 U Taq polymerase (Applied Biosystems) and inactivated water containing DEPC sufficient for a 20 μL final

reaction volume. A total of 45 cycles were performed; each cycle comprised 20 s at 94 °C, 20 s at 60 °C, and 30 s at 72 °C. There was an initial phase of denaturation at 94 °C for 5 min and an end phase of extension at 72 °C for 7 min.

RNA interference

RNAi was performed according to the manufacturer's instructions (Invitrogen set of 3 RNAi for pannexin-1). Briefly, mouse macrophages were treated with 2 μg/3 mL pannexin-1 interfering RNA using 4 μL/1 mL Lipofectamine 2000 reagent (Invitrogen) in Opti-MEM serum-free medium. After 16 h, the transfection reagents were removed and replaced by RPMI 1640 medium 10 % SFB; 24 h later, the experiments were performed.

Statistics

The result of each experiment is shown as the mean±SEM for the permeabilization assays and mean±SD for the FACS analysis. Data represent means of at least three independent experiments in triplicate. To test if the results fit a Gaussian distribution, the D'Agostino and Pearson's normality test was adopted. If the data fit a Gaussian distribution, we used a parametric test (ANOVA) with Bonferroni post hoc; if not, we used a nonparametric test (Kruskal–Wallis) with Dunn post hoc. Tests were two-tailed. The tests used are specified in figure legends. Differences were considered significant at $p<0.05$. Statistical and graphical analyses were performed using GraphPad Prism version 5.00 for Windows (GraphPad Software, San Diego, CA, USA).

Results

Hemichannel antagonists do not inhibit macroscopic currents associated with P2X7R

Mouse macrophages natively expressing P2X7R were used to test whether known gap junction antagonists could block the

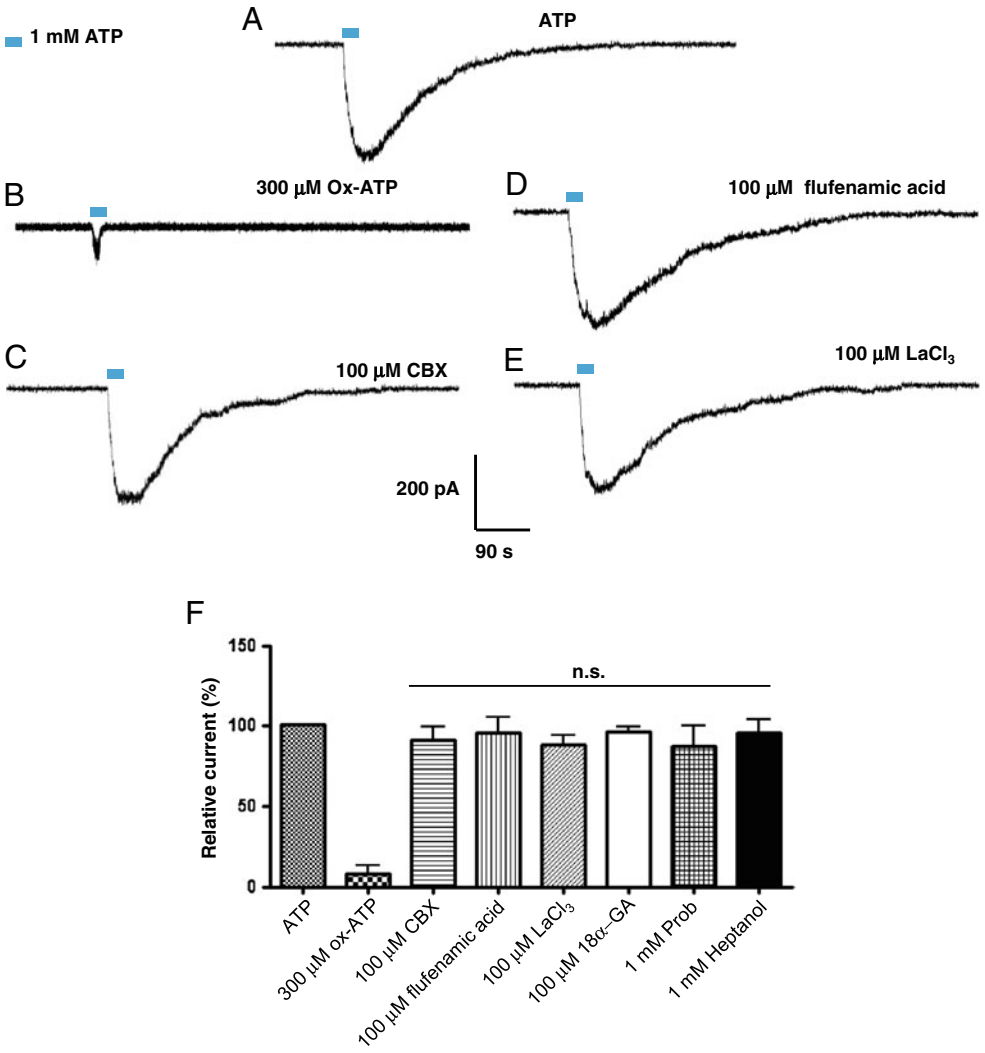

Fig. 1 Macroscopic ionic currents are not influenced by gap junction antagonists. **a** Current generated by the activation of the mouse P2X7R after addition of 1 mM ATP for 30 s in a whole-cell patch clamp. **b** Current blockage by preincubation (50 min) of 300 μM ox-ATP before stimulation with 1 mM ATP. Application of **c** 100 μM CBX, **d** 100 μM flufenamic acid, or **e** 100 μM $LaCl_3$ before activation of the mouse P2X7R with ATP. **f** Relative ATP-induced currents during drug application are indicated on the abscissa as a percentage of the mean current without drug application. All cells were stimulated by ATP prior application of ATP+ blocker, and then normalized the second recording by the first one. The *bar graphs* are representative of 5–10 experiments performed on different days (mean±SD). Data are normalized relative to 1 mM ATP treatment alone in whole-cell patch-clamp experiments. *Bars* represent ATP application for 30 s

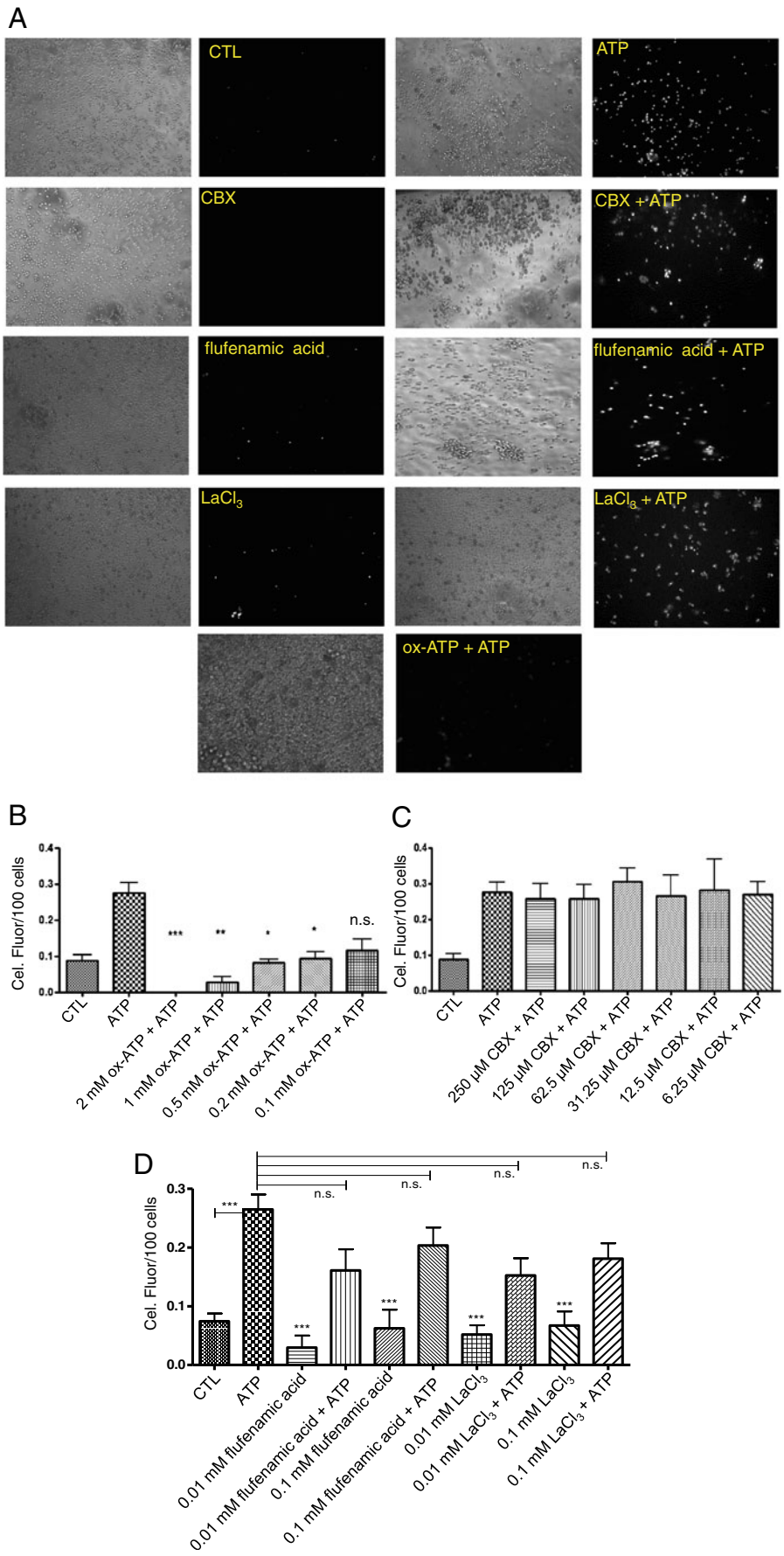

Fig. 2 Permeabilization assay with gap junction antagonists in rat peritoneal macrophages. **a** Permeabilization assays with 1 mM ATP, 300 μM ox-ATP (a known irreversible P2X7R antagonist), or 100 μM of the gap junction antagonists CBX, flufenamic acid, or $LaCl_3$. The *left panels* are the contrast phase, and the *right panels* represent fluorescence, showing EB uptake. **b**, **c** Quantification of the fluorescence within a field, with a mean of 100 cells per square treated with P2X7 antagonists: 0.1, 0.2, 0.5, 1.0, and 2.0 mM ox-ATP; 6.25, 12.5, 31.25, 62.5, 125, and 250 μM CBX. (D) Quantification of the fluorescence within a square, with a mean of 100 cells per square treated with 0.01 and 0.1 mM of the gap junction antagonists flufenamic acid and $LaCl_3$. All experiments were done at least in three different days and in triplicates, and the error bars are the mean of all measurements (nine squares per triplicate). Kruskal–Wallis with Dunn post hoc analyses were performed on the raw data (see "Materials and methods"): $*p<0.05$, $**p<0.01$, and $***p<0.001$ compared to the ATP group. Experiments were performed in triplicate, and quantification was performed on at least on three different days. *Bars* represent mean ± SEM

pore associated with P2X7R. Our first step was to study the macroscopic current associated with P2X7R activation using whole-cell patch clamp recordings. Macroscopic currents were recorded in mouse macrophages before, during, and after the application of 1 mM ATP to the bath with a holding potential of −60 mV (Fig. 1a). As expected, ionic currents were blocked by the P2X7R antagonist ox-ATP (300 μM, Fig. 1b). However, currents were unaffected by the application of 100 μM CBX (Fig. 1c), 100 μM flufenamic acid (Fig.1d), or 100 μM $LaCl_3$ (Fig. 1e). Figure 1f represents five to ten macroscopic currents observed on at least three different days. All recordings were normalized relative to the response to ATP, which was defined as maximal.

Peritoneal macrophages (unactivated and activated with LPS) were used to investigate the voltage dependence of the hemichannels, using steps from a holding potential of −80 mV to voltages between −120 and +80 mV following Valiunas and Weingart (2000). Supplementary Fig. 1 shows the ionic current obtained as a function of the applied voltage (*I–V*). For Supplementary Figs. 2–4, the holding potential was set to −80 mV, and voltage ramps were applied from −120 to +80 mV over 10 s (16 mV/s), with 40-s intervals between ramps. Voltage steps and ramps applied to LPS-activated macrophages and J774 cells seem to favor ionic currents at positive potentials and physiological Ca^{2+} concentrations, resembling the behavior of pannexin-mediated

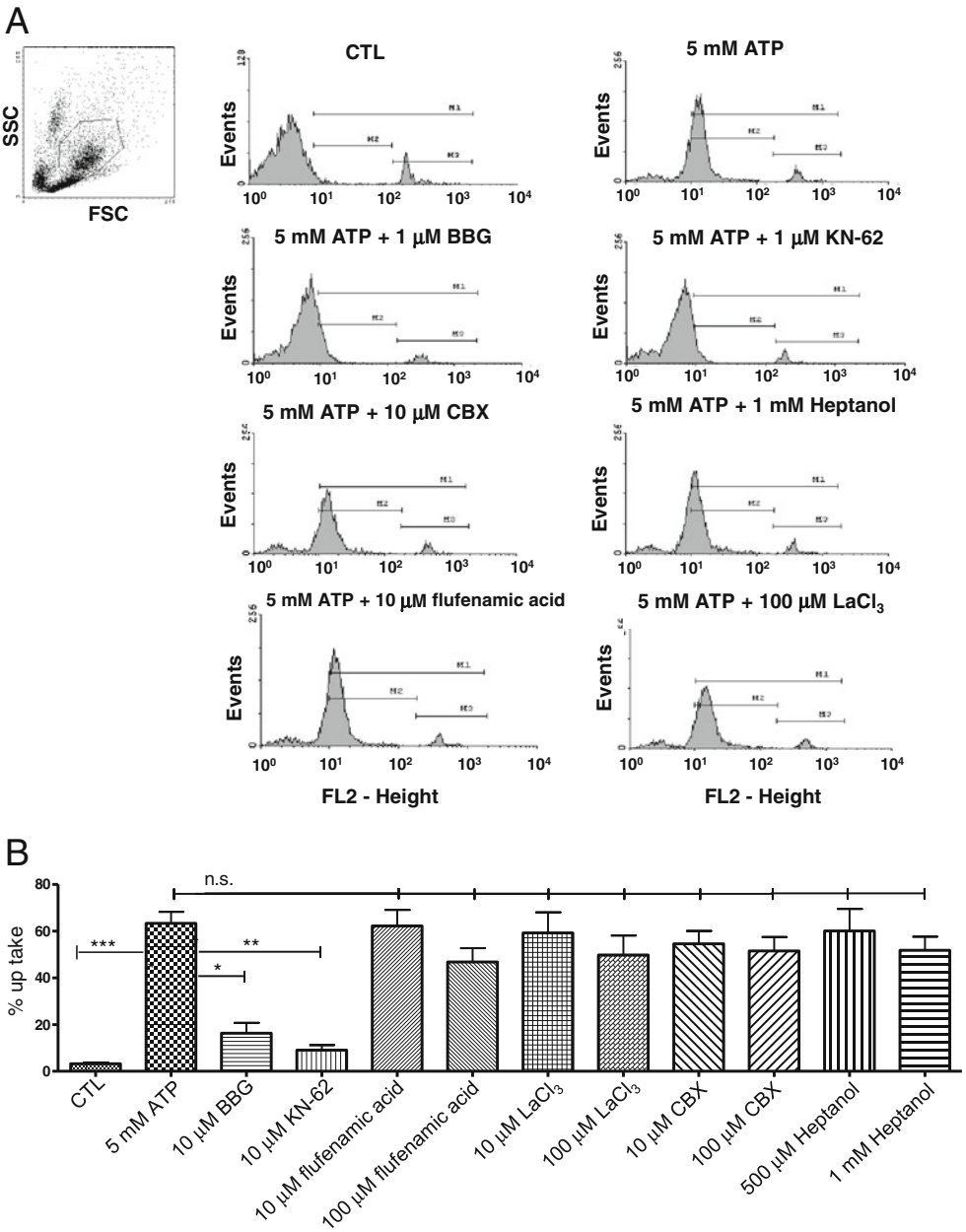

Fig. 3 FACs analysis of dye uptake in peritoneal mouse macrophages. P2X7R antagonists or gap junction antagonists were incubated for 15 min prior addition of 5 mM ATP. **a** P2X7R antagonists (BBG and KN-62) prevented the right shift of the curve compared to the 5 mM ATP control experiment, corresponding to an increase in fluorescence. Gap junction antagonists (CBX, heptanol, Acid flufenamic and LaCl3) did not block the increase in fluorescence represented by the right shift of the curves. **b** Dye uptake quantification of the means from different measurements in percentage versus antagonists. Kruskal–Wallis with Dunn post hoc analyses were performed on the raw data (see "Materials and methods"): *$p<0.05$, **$p<0.01$, and ***$p<0.001$. Experiments were performed in three different days and each experiment was done in triplicate. *Bars* represent mean±SD

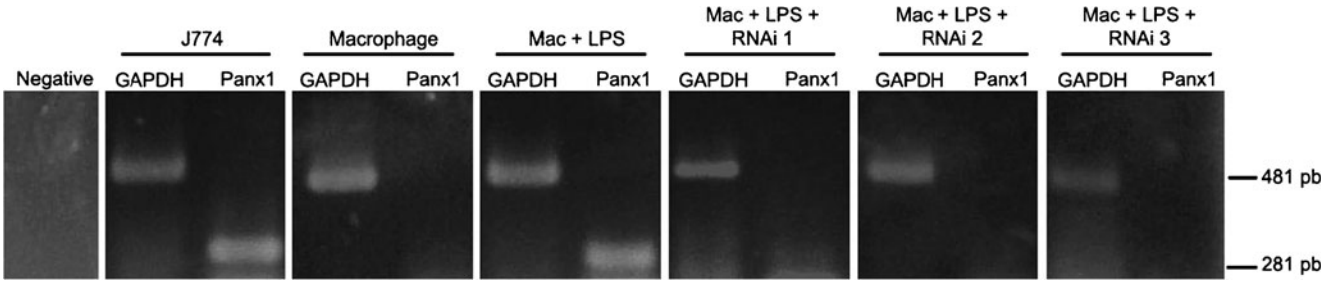

Fig. 4 Pannexin-1 (Panx1) expression in macrophages (Mac), as determined by RT-PCR. The J774.G8 cell line was used as a positive control for Panx1 mRNA expression, and constitutively expressed GAPDH mRNA was used as the positive control for each sample. Macrophages only display Panx1 mRNA expression after stimulation with LPS (Mac+LPS), and the expression of Panx1 is blocked by Panx1 RNAi constructs. *Negative* mock reaction for the RT-PCR reaction

currents (Supplementary Figs. 2 and 3). In peritoneal macrophages activated with LPS and J774 cells, currents were attenuated but not blocked by $LaCl_3$ or flufenamic acid, which are nonselective connexin antagonists. CBX (in the range of 1–25 μM), Prob (1 mM), and Mef (1 μM) are considered pannexin antagonists (Supplementary Fig. 2 and 3). All five compounds, however, reduced the ionic currents, confirming that the ionic current generated at positive membrane potentials, in activated peritoneal macrophages and J774 cells, is due to the opening of pannexin-1 channels. The voltage protocol was also applied to nonactivated mouse peritoneal macrophage (Supplementary Fig. 4). Among 25 nonactivated macrophages tested at different days, only two presented a discrete response (lower than 1–5 % of the maximum ionic current amplitude recorded in activated macrophages, data not shown), indicating that pannexin-1 is not functional in nonactivated macrophages.

Hemichannel antagonists do not inhibit dye uptake mediated by P2X7R in macrophages

We next tested the effects of hemichannel antagonists on membrane permeabilization associated with P2X7R pore activation in rat macrophages. The results are summarized in Fig. 2, in which "control" indicates the absence of drugs. When exposed to 1 mM ATP (5 min preincubation), most cells were permeable to the fluorescent dye. A 50-min preincubation of 300 μM ox-ATP blocked uptake of EB (50 ng/mL) in a significant, dose-dependent manner (Fig. 2a, b). A 5-min preincubation with the gap junction antagonists CBX, flufenamic acid, and $LaCl_3$ (10 or 100 μM) prior to 10 min of 1 mM ATP treatment did not block ATP-induced permeabilization (Fig. 2a–d). Alternatively, we induced blockage of connexin hemichannels by decreasing the intracellular pH with acetate (Supplementary Fig. 5). Therefore, there was no inhibition of the dye uptake elicited by ATP.

Uptake results were confirmed by FACS analysis of mouse macrophages. The gate in the FACS analysis was defined based on the morphology of cells in forward and side scatters. The test compounds used in the permeabilization protocols were included in these assays (Fig. 3). PI was employed as a fluorescent dye instead of EB. As a negative control, 50 ng/mL PI was added in the presence of saline. Approximately 65 % of the cells displayed 5 mM ATP-induced permeabilization (Fig. 3a). The murine P2X7R antagonists BBG and KN-62 blocked the effect of 5 mM ATP (Fig. 3a, b). By contrast, none of the gap junction antagonists tested (10 μM CBX, 10 μM flufenamic acid, 1 mM heptanol, and 100 μM $LaCl_3$) were able to significantly decrease the PI uptake induced by ATP (Fig. 3a, b). These results are summarized in Fig. 3b.

Because hemichannel antagonists did not have an effect on mouse macrophages, we performed reverse transcriptase PCR (RT-PCR) to verify the presence of pannexin-1 messenger RNA (mRNA). Surprisingly, primary cultures of mouse macrophages did not express pannexin-1 mRNA. We therefore activated the cells with LPS (24 h), after which pannexin-1 was upregulated (Fig. 4).

Pannexin-1 knockdown does not affect dye uptake

As hemichannel antagonists can be nonselective in some cases, we used 24 h of LPS activation to upregulate pannexin-1, then treated the cells with RNAi to knock down

Fig. 5 Dye uptake assay in peritoneal mouse macrophages treated with RNAi for Panx1. Macrophages were incubated with LPS for 24 h. **a** The cells were then transfected with interfering RNAis to knock down Panx1. After a 16-h incubation with RNAis in the presence of LPS, the cells were washed, and the Optimem medium was replaced by RPMI 10 % SFB. After 24 h, the cells were incubated in the presence or absence of BzATP (500 μM) for 15 min, followed by 5 min in the presence of PI. The *left panels* represent the contrast phase, and the *right panels* represent fluorescence, showing PI uptake. **b** Fluorescence was quantified according to the previously cited protocol. All experiments were done at least in three different days and in triplicates, and the errors are the mean of all measurements. Kruskal–Wallis with Dunn post hoc analyses were performed on the raw data (see "Materials and methods"): $*p<0.05$, $**p<0.01$, and $***p<0.001$ compared to the BzATP group. Lipof (as lipofectamine internal control). Experiments were performed in triplicate, and the quantification was performed on five different days. *Bars* represent mean ± SEM

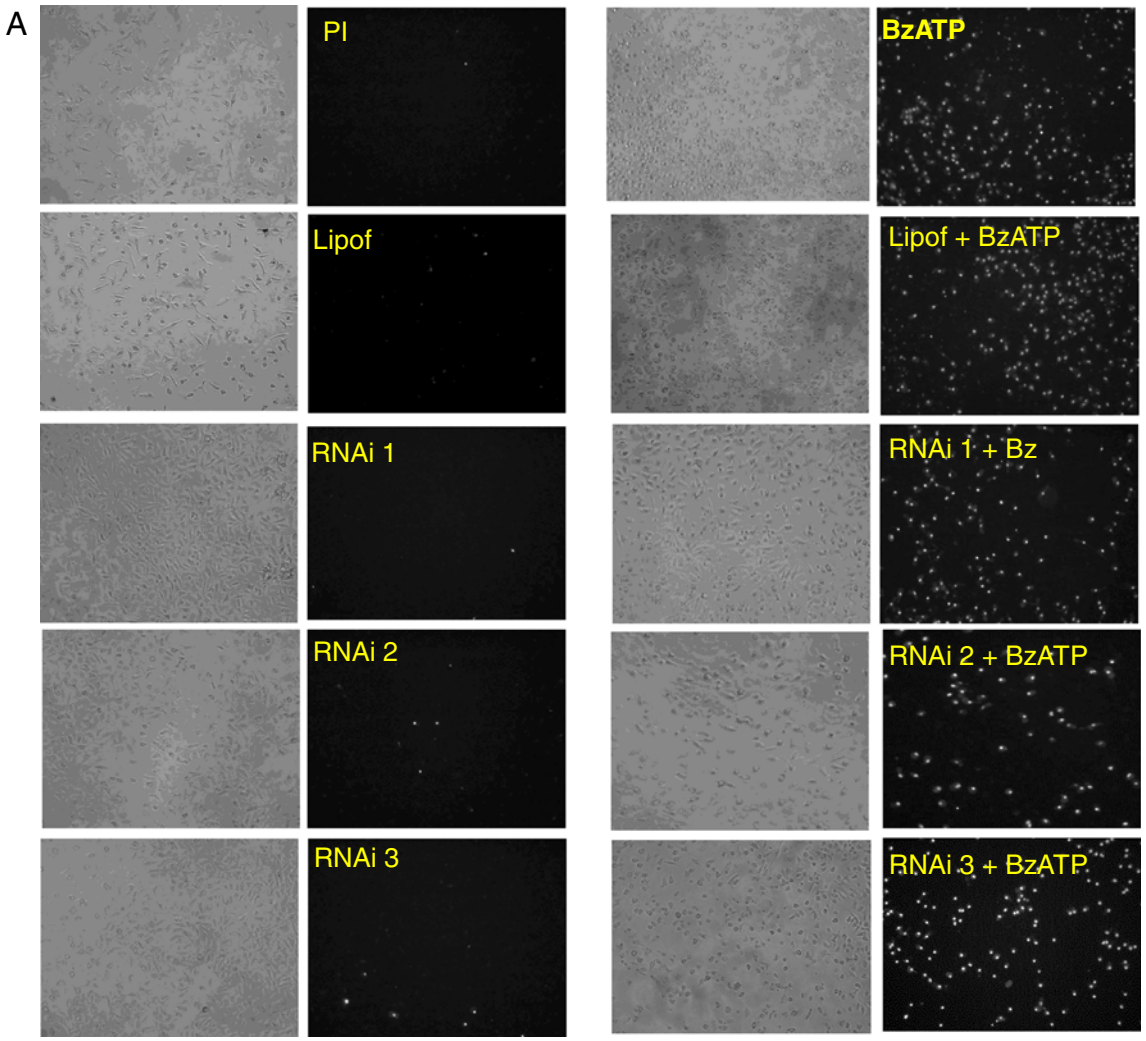

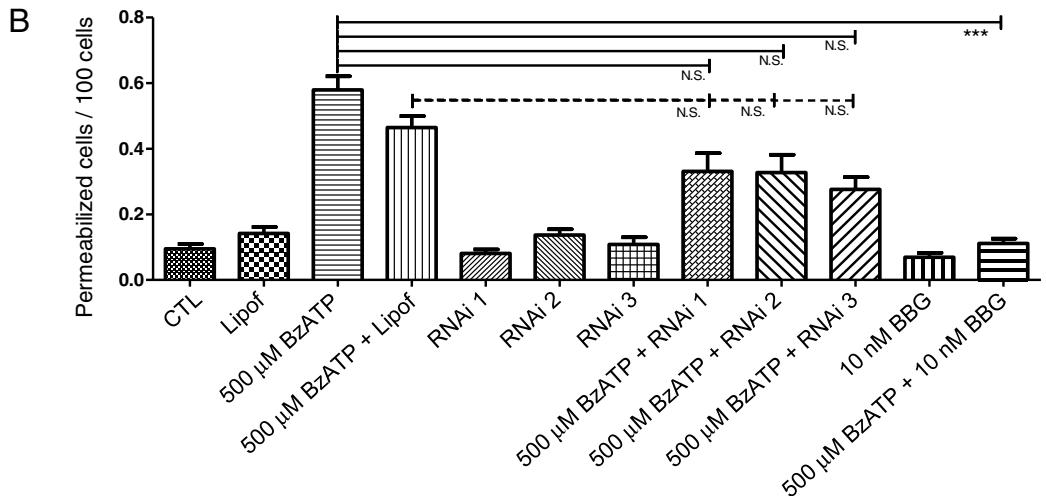

this protein. As shown in Fig. 4, pannexin expression was abolished by the interfering RNAis. Next, a dye uptake assay was performed with a similar protocol: the cells were activated by LPS and treated with RNAis. However, we used BzATP as an agonist because its potency in P2X7R is higher than that of ATP. Knockdown of pannexin-1 did not abrogate dye uptake elicited by BzATP in mouse macrophages (Fig. 5). In this context, we attempted to inhibit dye uptake in activated mouse macrophages with inhibitors reported to be specific for pannexin-1. Mef and Prob were

added 5 min prior to the application of ATP. Concentrations previously reported to induce pannexin-1 antagonism (10 and 100 nM Mef and 2 mM Prob) failed to inhibit dye uptake (Fig. 6) (Iglesias et al. 2008, 2009a, b; Silverman et al. 2009). Our data suggest that pannexin-1 does not contribute to the P2X7R-associated pore in primary cultures of macrophages, even after LPS activation.

Discussion

The main conclusion of our study is that pannexin-1 pore is not associated with P2X7R in peritoneal macrophages.

A high extracellular concentration of ATP acting on P2X7R leads to the opening of a nonselective, highly permeable pore (Rassendren et al. 1997b). The question addressed in the current study concerns the components of the pore triggered by P2X7R activation. Beyer and Steinberg (1991) suggested that the gap junction Cx43 could be the P2X7R activated pore, but this hypothesis was contradicted by Alves et al. (1995) with P2X7R knockout mice. Recently, it has been suggested that the pore may consist of hemichannels of pannexins (Pelegrin and Surprenant 2007). The reasoning relies mostly on the permeability limits of connexin hemichannels, which are similar to that of the P2X7 pore (1 kDa).

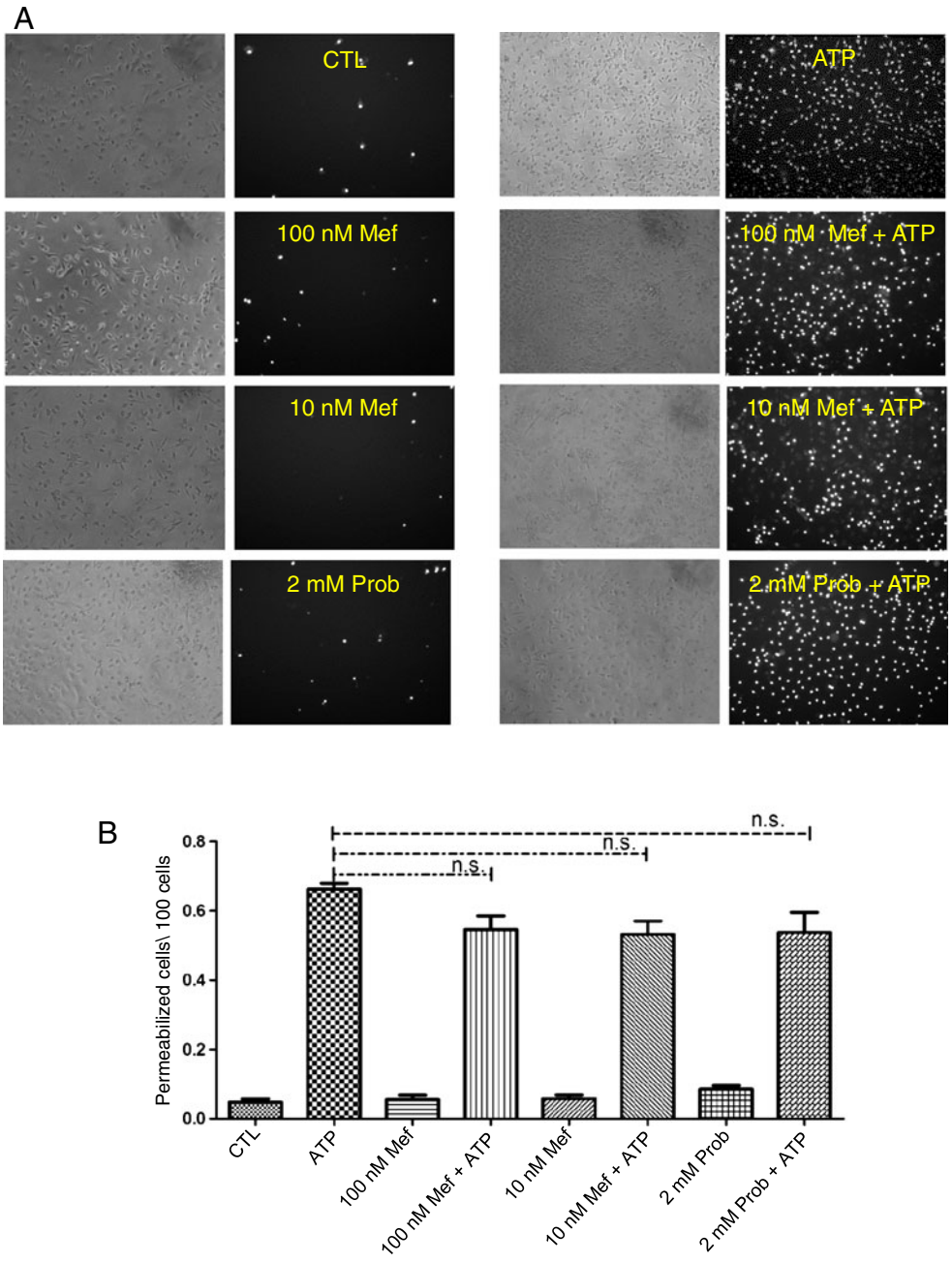

Fig. 6 Dye uptake assay in activated peritoneal mouse macrophages treated with Mef and Prob for inhibition of Panx1. **a** Permeabilization assays with 5 mM ATP, 100 or 10 nM Mef, or 2 mM Prob (Panx1 antagonists). The *left panels* represent the contrast phase, and the *right panels* display the fluorescence, showing ethidium bromide uptake. **b** Quantification of the fluorescence within a square, with a mean of 100 cells per square treated with 100 or 10 nM Mef and 2 mM Prob (Panx1 antagonists). All experiments were done at least in three different days and in triplicates, and the *bars* are the mean of all measurements. Kruskal–Wallis with Dunn post hoc analyses were performed on the raw data (see "Materials and methods"): $*p<0.05$, $**p<0.01$, and $***p<0.001$ compared to the ATP group. Experiments were performed in triplicate, and quantification was repeated on at least in five different days. *Bars* represent mean±SEM

Suadicani et al. (2006) demonstrated that gap junction antagonists inhibit dye uptake triggered by ATP in an astrocyte cell line stably transfected with rat P2X7R. Dye uptake was inhibited in the presence of well-known hemichannel antagonists such as heptanol, octanol, CBX, Mef, and flufenamic acid, suggesting that hemichannels of pannexin could contribute to the P2X7R-associated pore (Bruzzone et al. 2003; Iglesias et al. 2009b).

Pelegrin and Surprenant (2006) used molecular biology- and pharmacology-based approaches to demonstrate that the pore-like complex associated with P2X7R might be pannexin. In addition, they demonstrated that the ATP-induced current is not inhibited by Pan small interfering RNA (siRNA), pannexin-1 inhibiting peptide, or CBX. They also failed to completely block the dye uptake activated by ATP (Pelegrin and Surprenant 2006). Moreover, Qu et al. (2011) demonstrated that bone marrow-derived macrophages lacking pannexin do not exhibit decreased dye uptake upon ATP stimulation. This evidence suggests the participation of other pores or the opening of different pores in sequential cascades induced by P2X7R activation. Accordingly, Locovei et al. (2007) observed that pannexin-1 siRNA only partially blocks P2X7R-mediated pore-like formation. They attributed this to a nonspecific leakage or an unidentified pathway. They also demonstrated that CBX blocked pannexin-1 hemichannel activity. By contrast, the same research group (Ma et al. 2009) used HEK293 cells transfected with pannexin-1 to demonstrate that ATP and other nucleoside triphosphates (UTP and GTP) inhibit pore-like formation in a fashion similar to that observed after treatment with CBX.

In addition, pannexin-1 hemichannel activity but not connexin hemichannel activity is inhibited by low concentrations of CBX, with an IC_{50} in the range of 5 μM (Bruzzone et al. 2005). The same research group also demonstrated that pannexin-1 is unaffected by third-generation gap junction antagonists such as flufenamic acid and heptanol, which have been suggested for use as tools for an initial dissection of connexin and pannexin hemichannels. Contradicting this report is the evidence (Locovei et al. 2007) that P2X7R pore-like formation and/or pannexin-1 activity (ionic current) were blocked by Mef, CBX, and flufenamic acid. The authors suggested that Mef is a selective pannexin-1 antagonist.

These discrepancies in the pharmacological and/or genetic blockade of pannexin-1 hemichannels associated with inhibition of dye uptake suggest several possibilities. The first is related to the identity of the protein associated with the P2X7R pore. According to the pharmacological data described above, it is too early to confirm pannexin as the protein responsible for the formation of pore-like structures. Moreover, because the gap junction antagonists are not selective, we cannot exclude the possibility that these compounds are acting on an as-yet undescribed protein or on a known protein that is activated under conditions we have not studied.

Electrophysiological experiments in which CBX or heptanol were applied before ATP application revealed that both gap junction antagonists were unable to reduce the current due to the P2X7R-associated pore. Corroborating our hypothesis, the existence of two different pores was recently demonstrated in macrophages, namely, an anionic pore that allows the passage of LY and a cationic pore that allows the passage of EB (Schachter et al. 2008). In addition, in a primary macrophage culture, gap junction antagonists were not able to block the P2X7R pore. Yan et al. (2008) observed that CBX did not alter the current responses to BzATP in HEK293 cells expressing P2X7R. Furthermore, the uptake of YO-PRO in a primary culture of mouse astrocytes is not blocked by flufenamic acid or 18α-GA (Nagasawa et al. 2009). The P2X7R channel has been recently demonstrated to dilate under physiological ion concentrations, leading to the generation of a biphasic current. This process is controlled by residues near the intracellular side of the channel pore, independent of the expression of pannexin-1 channels. Nevertheless, Riedel et al. 2007 provided striking evidence demonstrating that the P2X7R pore does not dilate, thus contradicting this previous study.

These conflicting results regarding the P2X7R pore raise the question: Is only one entity responsible for this pore? Previously published data suggest the possible existence of more than one "pore protein," depending on the type, species, and manipulation of the cell (for example, transfection). In addition, P2X7R could potentially act through different "pore proteins" simultaneously. In this context, Cankurtaran-Sayar et al. (2009) recently demonstrated that both HEK-293 cells transfected with rat P2X7R and RAW 264.7 cells took up cationic (PI) and anionic (LY) fluorescent dyes after stimulation with 1 mM ATP. HEK-293 cells exhibited a Ca^{2+}-independent pathway for cationic dye permeation and another Ca^{2+}-dependent pathway for anionic dye permeation. RAW 264.7 cells were permeable to both dyes; chelation of intracellular Ca^{2+} slightly reduced the effect of ATP. However, an extracellular saline solution lacking Ca^{2+} reduced LY uptake without interfering with PI uptake. In addition, Schachter et al. (2008) demonstrated that transfected HEK-293 cells did not take up anionic dyes, in contrast to cationic dyes. They observed only Ca^{2+}-dependent anionic fluorescent dye uptake and Ca^{2+}-independent cationic dye uptake in peritoneal macrophages. Although they obtained distinct results in HEK-293 cells, all of these findings reinforce our conclusion that different pores are involved in P2X7R pore formation (Faria et al. 2009) and that different intracellular signaling pathways regulate these pores (Faria et al. 2005; Faria et al. 2009). Emphasizing this idea, Ma and collaborators demonstrated that pannexin-1 is an anion channel with a low unitary conductance (68 pS; Ma et al. 2012).

We therefore performed whole-cell experiments using peritoneal macrophages. We did not observe an effect of gap junction antagonists on P2X7R pore formation (Faria et al. 2005; Alves et al. 1999). Our experiments are not consistent with the participation of pannexin-1 in P2X7R pore formation in peritoneal macrophages. Pannexin-1 was functional in activating peritoneal macrophages after membrane depolarization with positive membrane potentials.

In the dye uptake assays in mouse macrophages, connexin and pannexin-1 antagonists and pannexin-1 siRNA all failed to inhibit ATP-induced pore formation via P2X7R activation (Figs. 2–6).

However, other groups have observed blockage of P2X7R pore formation by the pannexin antagonist CBX (1–10 μM), inhibitory peptides (Iglesias et al. 2008; Pelegrin and Surprenant 2007), or connexin antagonists (Suadicani et al. 2006; Iglesias et al. 2008).

The hypothesis that other pores participate in P2X7R pore formation may suggest that different intracellular signaling pathways occur in the same cell to activate a unique pore or pores. Taken together, our findings indicate that, in primary mouse or rat macrophage cultures, P2X7R does not associate with pannexin-1 to form the large conductance channels known as P2X7R pores.

Acknowledgments This work was supported by grants from IOC/FIOCRUZ, FAPERJ, and CNPq.

Conflict of interest The authors state no conflict of interest.

References

Alloisio S et al (2008) Functional evidence for presynaptic P2X7 receptors in adult rat cerebrocortical nerve terminals. FEBS Lett 582(28):3948–3953

Alves LA et al (1995) Functional gap junctions in thymic epithelial cells are formed by connexin 43. Eur J Immunol 25(2):431–437

Alves LA et al (1996) Are there functional gap junctions or junctional hemichannels in macrophages? Blood 88(1):328–334

Alves LA, Coutinho-Silva R, Savino W (1999) Extracellular ATP: a further modulator in neuroendocrine control of the thymus. Neuroimmunomodulation 6(1–2):81–89

Atkinson L et al (2004) Differential co-localisation of the P2X7 receptor subunit with vesicular glutamate transporters VGLUT1 and VGLUT2 in rat CNS. Neuroscience 123(3):761–768

Auger R et al (2005) A role for mitogen-activated protein kinase(Erk1/2) activation and non-selective pore formation in P2X7 receptor-mediated thymocyte death. J Biol Chem 280(30):28142–28151

Barbe MT, Monyer H, Bruzzone R (2006) Cell-cell communication beyond connexins: the pannexin channels. Physiology (Bethesda) 21:103–114

Bauer R et al (2005) Intercellular communication: the *Drosophila* innexin multiprotein family of gap junction proteins. Chem Biol 12(5):515–526

Bennett MV et al (1991) Gap junctions: new tools, new answers, new questions. Neuron 6(3):305–320

Beyer EC, Steinberg TH (1991) Evidence that the gap junction protein connexin-43 is the ATP-induced pore of mouse macrophages. J Biol Chem 266(13):7971–7974

Bosco D, Haefliger J-A, Meda P (2011) Connexins: key mediators of endocrine function. Physiol Rev 91(4):1393–1445

Bruzzone R, Dermietzel R (2006) Structure and function of gap junctions in the developing brain. Cell Tissue Res 326(2):239–248

Bruzzone R et al (2003) Pannexins, a family of gap junction proteins expressed in brain. Proc Natl Acad Sci U S A 100(23):13644–13649

Bruzzone R et al (2005) Pharmacological properties of homomeric and heteromeric pannexin hemichannels expressed in *Xenopus* oocytes. J Neurochem 92(5):1033–1043

Cankurtaran-Sayar S, Sayar K, Ugur M (2009) P2X7 receptor activates multiple selective dye-permeation pathways in RAW 264.7 and human embryonic kidney 293 cells. Mol Pharmacol 76(6):1323–1332

Cario-Toumaniantz C et al (1998) Non-genomic inhibition of human P2X7 purinoceptor by 17beta-oestradiol. J Physiol 508(Pt 3):659–666

Cockcroft S, Gomperts BD (1980) The ATP4+ receptor of rat mast cells. Biochem J 188(3):789–798

Contreras JE et al (2002) Metabolic inhibition induces opening of unapposed connexin 43 gap junction hemichannels and reduces gap junctional communication in cortical astrocytes in culture. Proc Natl Acad Sci U S A 99(1):495–500

Coutinho-Silva R, Persechini PM (1997) P2Z purinoceptor-associated pores induced by extracellular ATP in macrophages and J774 cells. Am J Physiol 273(6 Pt 1):C1793–C1800

Deuchars SA et al (2001) Neuronal P2X7 receptors are targeted to presynaptic terminals in the central and peripheral nervous systems. J Neurosci: Offic J Soc Neurosci 21(18):7143–7152

Evans WH, Martin PE (2002) Lighting up gap junction channels in a flash. Bioessays 24(10):876–880

Faria RX, de Farias FP, Alves LA (2005) Are second messengers crucial for opening the pore associated with P2X7 receptor? Am J Physiol Cell Physiol 288(2):C260–C271

Faria RX et al (2009) Pharmacological properties of a pore induced by raising intracellular Ca2+. Am J Physiol Cell Physiol 297(1):C28–C42

Ferrari D et al (1997) Extracellular ATP triggers IL-1 beta release by activating the purinergic P2Z receptor of human macrophages. J Immunol 159(3):1451–1458

Gudipaty L et al (2003) Essential role for Ca2+ in regulation of IL-1beta secretion by P2X7 nucleotide receptor in monocytes, macrophages, and HEK-293 cells. Am J Physiol Cell Physiol 285:C286–C299

Harris AL (2001) Emerging issues of connexin channels: biophysics fills the gap. Q Rev Biophys 34(3):325–472

Heppel LA, Weisman GA, Friedberg I (1985) Permeabilization of transformed cells in culture by external ATP. J Membr Biol 86(3):189–196

Humphreys BD et al (2000) Stress-activated protein kinase/JNK activation and apoptotic induction by the macrophage P2X7 nucleotide receptor. J Biol Chem 275(35):26792–26798

Iglesias R et al (2008) P2X7 receptor-Pannexin1 complex: pharmacology and signaling. Am J Physiol Cell Physiol 295(3):C752–C760

Iglesias R et al (2009a) Pannexin 1: the molecular substrate of astrocyte "hemichannels". J Neurosci 29(21):7092–7097

Iglesias R, Spray DC, Scemes E (2009b) Mefloquine blockade of Pannexin1 currents: resolution of a conflict. Cell Commun Adhes 16(5–6):131–137

Jacobson GM et al (2010) Connexin36 knockout mice display increased sensitivity to pentylenetetrazol-induced seizure-like behaviors. Brain Res 1360:198–204

Jiang LH et al (2005) N-methyl-D-glucamine and propidium dyes utilize different permeation pathways at rat P2X(7) receptors. Am J Physiol Cell Physiol 289(5):C1295–C1302

Ke HZ et al (2003) Deletion of the P2X7 nucleotide receptor reveals its regulatory roles in bone formation and resorption. Mol Endocrinol (Baltimore, Md) 17(7):1356–1367

Kim SY et al (2007) ATP released from beta-amyloid-stimulated microglia induces reactive oxygen species production in an autocrine fashion. Exp Mol Med 39(6):820–827

Li Q et al (2003) Cell-specific behavior of P2X7 receptors in mouse parotid acinar and duct cells. J Biol Chem 278(48):47554–47561

Locovei S et al (2007) Pannexin1 is part of the pore forming unit of the P2X(7) receptor death complex. FEBS Lett 581(3):483–488

Ma W et al (2009) Pharmacological characterization of pannexin-1 currents expressed in mammalian cells. J Pharmacol Exp Ther 328(2):409–418

Ma W et al (2012) Pannexin 1 forms an anion-selective channel. Pflugers Arch 463(4):585–592

Marcoli M et al (2008) P2X7 pre-synaptic receptors in adult rat cerebrocortical nerve terminals: a role in ATP-induced glutamate release. J Neurochem 105(6):2330–2342

Monif M et al (2009) The P2X7 receptor drives microglial activation and proliferation: a trophic role for P2X7R pore. J Neurosci 29(12):3781–3791

Nagasawa K, Escartin C, Swanson RA (2009) Astrocyte cultures exhibit P2X7 receptor channel opening in the absence of exogenous ligands. Glia 57(6):622–633

Pelegrin P, Surprenant A (2006) Pannexin-1 mediates large pore formation and interleukin-1beta release by the ATP-gated P2X7 receptor. EMBO J 25(21):5071–5082

Pelegrin P, Surprenant A (2007) Pannexin-1 couples to maitotoxin- and nigericin-induced Interleukin-1beta release through a dye uptake-independent pathway. J Biol Chem 282:2386–2394

Persechini PM et al (1998) Extracellular ATP in the lymphohematopoietic system: P2Z purinoceptors off membrane permeabilization. Braz J Med Biol Res 31(1):25–34

Qu Y et al (2011) Pannexin-1 is required for ATP release during apoptosis but not for inflammasome activation. J Immunol 186(11):6553–6561

Rassendren F et al (1997a) Identification of amino acid residues contributing to the pore of a P2X receptor. EMBO J 16(12):3446–3454

Rassendren F et al (1997b) The permeabilizing ATP receptor, P2X7. Cloning and expression of a human cDNA. J Biol Chem 272(9):5482–5486

Riedel T et al (2007) Kinetics of P2X7 receptor-operated single channels currents. Biophys J 92(7):2377–2391

Schachter J et al (2008) ATP-induced P2X7-associated uptake of large molecules involves distinct mechanisms for cations and anions in macrophages. J Cell Sci 121(Pt 19):3261–3270

Silverman WR et al (2009) The pannexin 1 channel activates the inflammasome in neurons and astrocytes. J Biol Chem 284(27):18143–18151

Steinberg TH et al (1987) ATP4+ permeabilizes the plasma membrane of mouse macrophages to fluorescent dyes. J Biol Chem 262(18):8884–8888

Suadicani SO, Brosnan CF, Scemes E (2006) P2X7 receptors mediate ATP release and amplification of astrocytic intercellular Ca2+ signaling. J Neurosci 26(5):1378–1385

Surprenant A et al (1996) The cytolytic P2Z receptor for extracellular ATP identified as a P2X receptor (P2X7). Science 272(5262):735–738

Valiunas V (2002) Biophysical properties of connexin-45 gap junction hemichannels studied in vertebrate cells. J Gen Physiol 119(2):147–164

Valiunas V, Weingart R (2000) Electrical properties of gap junction hemichannels identified in transfected HeLa cells. Pflugers Arch 440(3):366–379

Valiunas V et al (1999) Electrophysiological properties of gap junction channels in hepatocytes isolated from connexin32-deficient and wild-type mice. Pflugers Arch 437(6):846–856

Virginio C et al (1999a) Kinetics of cell lysis, dye uptake and permeability changes in cells expressing the rat P2X7 receptor. J Physiol 519(2):335–346

Virginio C et al (1999b) Pore dilation of neuronal P2X receptor channels. Nat Neurosci 2(4):315–321

Yan Z et al (2008) The P2X7 receptor channel pore dilates under physiological ion conditions. J Gen Physiol 132(5):563–573